Paper

Comparison of Four Resonant Topologies Based on Unified Design Procedure for Capacitive Power Transfer

Takehiro Imura*a) Member, Kenta Suzuki** Non-member, Katsuhiro Hata** Member, Yoichi Hori** Fellow

(Manuscript received Jan. 00, 20XX, revised May 00, 20XX)

This study analyzes and evaluates four transmission characteristics of the capacitive power transfer (CPT) with resonance coupling. A constant voltage source is used under all conditions. The target compensation topologies for the investigation are series-series (SS), series-parallel (SP), parallel-series (PS) and parallel-parallel (PP) topologies. The analysis results under the unified conditions describe the five transmission characteristics: (a) the equivalent maximum efficiency in four topologies, (b) the squared lower output power of the coupling coefficient of PS and PP topologies compared with those of SS and SP topologies, (c) the squared lower optimal loads of the coupling coefficient of SS and PS topologies compared with those of SP and PP topologies, (d) the constant unit power factor (CUPF) characteristics from the source in four topologies, (e) the constant current (CC) characteristics in SS and PP topologies, and the constant voltage (CV) characteristics in SP and PS topologies at the load variation around the optimal load. From these evaluations, both SS and SP topologies, which are superior in terms of the output power, are recommended when using the voltage source. Finally, the powering experiment in SS and SP topologies shows the effectiveness of these evaluations.

Keywords : Wireless power transfer, capacitive power transfer, SS topology, SP topology, PS topology, PP topology

1. Introduction

Wireless power transfer (WPT) has attached world-wide attention as a method to solve the problems of cable charging such as abrasion and disconnection[1]-[6].WPT methods are classified into two major fields: inductive power transfer (IPT) via alternating magnetic field and capacitive power transfer (CPT) via alternating electric field. IPT couplers consist of a pair of coils, but the litz wire reducing the high frequency resistance and ferrite core maintaining the strong coupling between the couplers are additionally employed. These are prone to make the expensive and heavy system. Conversely, CPT enables lower-cost and lighter-weight implementation because couplers consist of metal plates only. Also, because of the transmission with the electric field, CPT can avoid the eddy current on the foreign metal object between couplers and excludes the lowering efficiency and risk of temperature rise. Furthermore, the flexibility of coupler shape is also its noteworthy advantage. Utilizing these advantages, CPT is applied to various charging applications for the soccer robot[7], LED driver[8], biomedical implant[9], synchronous machines[10] and electric vehicle[11].

On the other hand, the difficulty of the high-power transmission in CPT is known due to the extremely small capacitance between couplers[12]. However, recent study which employ the double sided LCLC-compensated topology[13] succeeded in high efficiency of 90 % and high power of 2.4 kW transmission at long distance of 150 mm. Therefore, the industrial applications of CPT independent on distance is expected. Also, the simple compensation topologies with less number of elements of two has been widely analyzed[14]-[18]. About series-series (SS) topology as one of them, the values of transmission efficiency, output power and the optimal load which achieves the maximum efficiency are shown [17]. In addition, it is described that the properly designed compensation inductors provide the load-independent constant unit power factor (CUPF) from the source and constant current (CC) characteristics. About SS and series-parallel (SP) topologies, the equivalent target values of their transmission efficiency and output power, and the lower optimal load of SS topology compared with that of SP topology are explained when primary and secondary sides input reactance are zero[16]. About SS and parallel-parallel (PP) topologies, the equivalent target values of their transmission efficiency are explained[18]. Although, it is still difficult to select the appropriate topology because the circuit analysis and understanding of the transmission characteristics are not enough than IPT where it is discussed under unified compensation condition[19]. The reasons are as follows: (i) unexamined parallel-series (PS) topology, (ii) insufficient evaluation of the transmission characteristics in SP and PP topologies because CC and constant voltage characteristics (CV) are not discussed[16], [18]. (iii) Non-uniform compensation inductor design for each article. For example, the resonances in reference (16) are designed so that the input reactance of the secondary as well as the primary side is zero, while in reference (17) and (18), the resonances are simply made to resonate at the plate capacitance C and resonant coil L. These compensation methods are different from the gyrators and ideal transformer methods in this paper. (iv) ignoring the loss resistances for the evaluation of the output power, CUPF, CC and CV characteristics.

Therefore, this paper fairly compares four topologies by evaluating the transmission characteristics under the unified inductor design and the optimal load. Here, the inductors for all topologies are designed based on constituting the gyrator and ideal transformer networks to be expected for the CUPF, and CC or CV characteristics. In IPT, it is said that the analysis by these networks can describe transmission characteristics of each topology graphically[20]. Furthermore, this paper evaluates five important transmission characteristics: (a) transmission efficiency, (b) output power, (c) optimal load, (d) CUPF characteristics, (e) CC and CV

a) Correspondence to: Takehiro Imura. E-mail: imura.takehiro@rs.tus.ac.jp
* Tokyo University of Science.
** The University of Tokyo.

characteristics. Based on these evaluations, the criterion for the selection of the compensation topology for each application are presented. Finally, the powering experiment in SS and SP topologies shows the effectiveness these evaluations.

2. CPT with resonance coupling

2.1. CPT coupler

Typical CPT couplers consist of four metal plates Plate1–Plate4 horizontally arranged such as Fig. 1. Plate1, 2 are on the primary side with the power supply, Plate3, 4 are on the secondary side with the load. The circuit diagram based on capacitances between each plate $C_{12} - C_{34}$ is described in Fig. 2(a). Also, this is converted into the π type circuit diagram in Fig. 2(b)[22]. The self-capacitances C_1, C_2 and mutual capacitance C_m are expressed as follows:

$$C_1 = C_{12} + \frac{(C_{13}+C_{14})(C_{23}+C_{24})}{C_{13}+C_{14}+C_{23}+C_{24}} \quad (1)$$

$$C_2 = C_{34} + \frac{(C_{13}+C_{14})(C_{23}+C_{24})}{C_{13}+C_{14}+C_{23}+C_{24}} \quad (2)$$

$$C_m = \frac{C_{24}C_{13}-C_{14}C_{23}}{C_{13}+C_{14}+C_{23}+C_{24}} \quad (3)$$

$$k = \frac{C_m}{\sqrt{C_1 C_2}} \quad (4)$$

where k is defined as a coupling coefficient representing the strength of coupling between the primary and secondary sides.

2.2. Compensation topology

In WPT, the high-efficiency and high-power transmission needs compensation by the external elements. The element design in this paper focuses on two of the compensation inductors conditions and optimal load conditions to maximize the transmission efficiency.

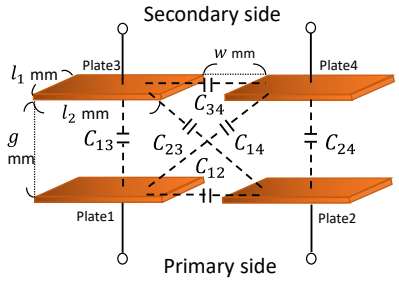

Fig. 1. Typical structure of CPT couplers

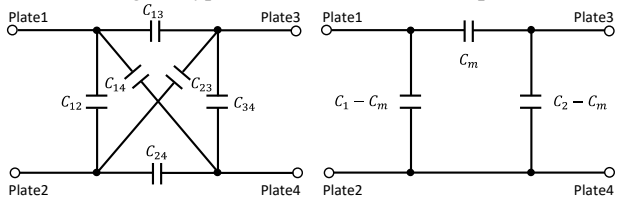

(a) Structure circuit (b) π-type circuit

Fig. 2. Equivalent circuit diagram of CPT couplers

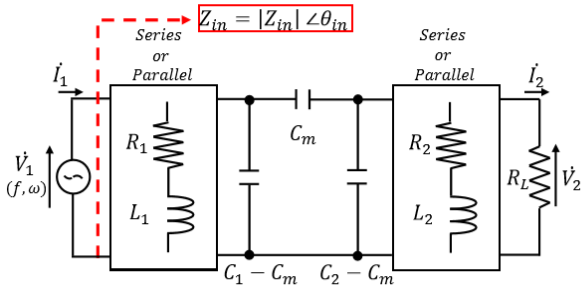

Fig. 3. Circuit diagram of CPT with resonance coupling

The examined compensation topologies are SS, SP, PS and PP topologies described in Fig. 3. There are named based on how the inductors are connected on each side, series (S) or parallel (P). Here, L_1, L_2 are the inductances and R_1, R_2 are the equivalent series resistances (ESR) of the compensation inductors. The quality factors of the inductors are defined as follows.

$$Q_1 = \frac{\omega L_1}{R_1}, Q_2 = \frac{\omega L_2}{R_2} \quad (5)$$

$\dot{V}_1$, $\dot{V}_2$ are the input and output voltages, $\dot{I}_1$, $\dot{I}_2$ are the input and output currents. R_L is load resistance and f, ω are the operating frequency and angular frequency.

3. Compensation inductor design ($R_1 = R_2 = 0$)

This section derives the compensation inductor conditions under $R_1 = R_2 = 0$. The design method based on the gyrator and ideal transformer networks is employed to obtain CUPF, and CC or CV characteristics.

3.1. Gyrator and ideal transformer characteristics

The gyrator is a circuit network satisfying $\dot{A} = \dot{D} = 0$ in the circuit equation of eq. (6)[20),(21)]. Also, the cascade connection of even number of gyrators satisfy $\dot{B} = \dot{C} = 0$.

$$\begin{bmatrix}\dot{V}_1 \\ \dot{I}_1\end{bmatrix} = \begin{bmatrix}\dot{A} & \dot{B} \\ \dot{C} & \dot{D}\end{bmatrix}\begin{bmatrix}\dot{V}_2 \\ \dot{I}_2\end{bmatrix} \quad (6)$$

When there is no loss resistance in the circuit, the condition of $\dot{A} = \dot{D} = 0$ provides the CUPF characteristics as shown in eq.(8) where Z_{in} is represented as real number and the CC characteristics as shown in eq.(10) where $|\dot{I}_2|$ is independent on R_L. These are collectively named as gyrator characteristics.

Also, the condition of $\dot{B} = \dot{C} = 0$ provides the CUPF characteristics as shown in eq.(12) where Z_{in} is represented as real number and the CV characteristics as shown in eq.(13) where $|\dot{V}_2|$ is independent on R_L. These are collectively named as ideal transformer characteristics.

$\dot{A} = \dot{D} = 0$: Gyrator characteristics

$$\begin{bmatrix}\dot{V}_1 \\ \dot{I}_1\end{bmatrix} = \begin{bmatrix}0 & \pm jZ_{01} \\ \pm j/Z_{01} & 0\end{bmatrix}\begin{bmatrix}\dot{V}_2 \\ \dot{I}_2\end{bmatrix} \quad (7)$$

$$Z_{in} = \dot{V}_1/\dot{I}_1 = Z_{01}^2 R_L \ (\cos\theta_{in} = 1) \quad (8)$$

$$|\dot{V}_2| = R_L/Z_{01}|\dot{V}_1| \quad (9)$$

$$|\dot{I}_2| = 1/Z_{01}\ |\dot{V}_1| \quad (10)$$

$\dot{B} = \dot{C} = 0$: Ideal transformer characteristics

$$\begin{bmatrix}\dot{V}_1 \\ \dot{I}_1\end{bmatrix} = \begin{bmatrix}\pm Z_{02} & 0 \\ 0 & \pm 1/Z_{02}\end{bmatrix}\begin{bmatrix}\dot{V}_2 \\ \dot{I}_2\end{bmatrix} \quad (11)$$

$$Z_{in} = \dot{V}_1/\dot{I}_1 = Z_{02}^2 R_L \ (\cos\theta_{in} = 1) \quad (12)$$

$$|\dot{V}_2| = 1/Z_{02}|\dot{V}_1| \quad (13)$$

$$|\dot{I}_2| = 1/Z_{02}R_L\ |\dot{V}_1| \quad (14)$$

In subsequent analysis, the compensation inductor conditions satisfying $\dot{A} = \dot{D} = 0$ or $\dot{B} = \dot{C} = 0$ are derived. For the simple analysis, the following parameters are employed.

$$\begin{cases} \alpha = 1 - \omega^2 L_1 C_1 (1 - k^2) \\ \beta = 1 - \omega^2 L_2 C_2 (1 - k^2) \\ \gamma = 1 + \omega^4 L_1 L_2 C_1 C_2 (1 - k^2) - \omega^2 (L_1 C_1 + L_2 C_2) \end{cases} \quad (15)$$

3.2. Design procedure

The F parameters $\dot{A} - \dot{D}$ of the circuit equation in SS topology are expressed as Table 1. Table 2 is under compensation condition.

Table 1 F parameter, compensation inductor conditions and gyrator and ideal transformer characteristics in each topology.

	SS topology	SP topology	PS topology	PP topology
$\dot{A}$	$\alpha C_2/C_m$	$-\gamma/\omega^2 L_2 C_m$	C_2/C_m	$-(1-\omega^2 L_2 C_2)/\omega^2 L_2 C_m$
$\dot{B}$	$\gamma/j\omega C_m$	$(1-\omega^2 L_1 C_1)/j\omega C_m$	$(1-\omega^2 L_2 C_2)/j\omega C_m$	$1/j\omega C_m$
$\dot{C}$	$j\omega C_m(1-k^2)/k^2$	$\beta C_1/j\omega L_2 C_m$	$\alpha C_2/j\omega L_1 C_m$	$-\gamma/j\omega^3 L_1 L_2 C_m$
$\dot{D}$	$\beta C_1/C_m$	C_1/C_m	$-\gamma/\omega^2 L_1 C_m$	$-(1-\omega^2 L_1 C_1)/\omega^2 L_1 C_m$
L_1	$1/\omega^2 C_1(1-k^2)$	$1/\omega^2 C_1$	$1/\omega^2 C_1(1-k^2)$	$1/\omega^2 C_1$
L_2	$1/\omega^2 C_2(1-k^2)$	$1/\omega^2 C_2(1-k^2)$	$1/\omega^2 C_2$	$1/\omega^2 C_2$
Z_{in}	$k^4/\omega^2 C_m^2 R_L(1-k^2)^2$	$C_m^2 R_L/C_1^2$	$C_2^2 R_L/C_m^2$	$\omega^2 C_m^2/R_L$
$\lvert\dot{V}_2\rvert$	$\omega C_m R_L(1-k^2)/k^2\lvert\dot{V}_1\rvert$	$C_1/C_m\lvert\dot{V}_1\rvert$	$C_m/C_2\lvert\dot{V}_1\rvert$	$\omega C_m R_L\lvert\dot{V}_1\rvert$
$\lvert\dot{I}_2\rvert$	$\omega C_m(1-k^2)/k^2\lvert\dot{V}_1\rvert$	$C_1/C_m R_L\lvert\dot{V}_1\rvert$	$C_m/C_2 R_L\lvert\dot{V}_1\rvert$	$\omega C_m\lvert\dot{V}_1\rvert$
Characteristics	Gyrator	Ideal Transformer	Ideal Transformer	Gyrator

Table 2 F parameter under compensation condition.

	SS topology	SP topology	PS topology	PP topology
$\dot{A}$	0	C_m/C_1	C_2/C_m	0
$\dot{B}$	$-k^2/j\omega C_m(1-k^2)$	0	0	$1/j\omega C_m$
$\dot{C}$	$j\omega C_m(1-k^2)/k^2$	0	0	$-j\omega C_m$
$\dot{D}$	0	C_1/C_m	C_m/C_2	0
Characteristics	Gyrator	Ideal Transformer	Ideal Transformer	Gyrator

$$\begin{cases} \dot{A}=\frac{C_2}{C_m}\alpha,\ \dot{B}=\frac{\gamma}{j\omega C_m} \\ \dot{C}=\frac{j\omega C_m(1-k^2)}{k^2},\ \dot{D}=\frac{C_1}{C_m}\beta \end{cases} \tag{16}$$

In SS topology, it is possible to satisfy only $\dot{A}=\dot{D}=0$ by appropriate design of compensation inductors as follows.

$$L_1=\frac{1}{\omega^2 C_1(1-k^2)},\ L_2=\frac{1}{\omega^2 C_2(1-k^2)} \tag{17}$$

The input impedances at this condition are shown in eq. (18). Also, the output voltage $|\dot{V}_2|$ and output current $|\dot{I}_2|$ are shown in eqs. (19), (20).

$$Z_{in}=\frac{k^4}{\omega^2 C_m^2 R_L(1-k^2)^2}\ (\cos\theta_{in}=1) \tag{18}$$

$$\left|\dot{V}_2\right|=\frac{\omega C_m R_L(1-k^2)}{k^2}\left|\dot{V}_1\right| \tag{19}$$

$$\left|\dot{I}_2\right|=\frac{\omega C_m(1-k^2)}{k^2}\left|\dot{V}_1\right| \tag{20}$$

Independent on R_L, Z_{in} is real and $|\dot{I}_2|$ is constant. Hence, it is shown that SS topology gains gyrator characteristics with the compensation inductor condition. Other topologies are also analyzed in the same procedure, and the results are listed in Table 1. They are understood that the SS, PP topologies satisfy $\dot{A}=\dot{D}=0$ and obtain the gyrator characteristics, and the SP, PP topologies satisfy $\dot{B}=\dot{C}=0$ and obtain the ideal transformer characteristics. Comparing only the compensation inductor conditions, PP topology with L_1 and L_2 independent on k has a little advantage. This is because the resonance deviation unlikely occurs even in dynamic systems where k varies depending on the target position.

4. Circuit analysis and evaluation ($R_1 \neq R_2 \neq 0$)

The transmission characteristics are evaluated, and topologies are compared by deriving the formulas of the transmission efficiency, output power, optimal load, input impedance, output current and output voltage. The details of the circuit analysis of only SS topology are shown, and formulas of other topologies are summarized in tables. For simple formulas, k in eq. (4), quality factors in eq. (5) and following parameters are employed.

$$\begin{cases} Q_{1\delta}=\frac{1+Q_1^2}{Q_1}, Q_{2\delta}=\frac{1+Q_2^2}{Q_2}, \delta_k=\frac{k^2}{1-k^2} \\ A_k=R_2Q_2+k^2R_LQ_1 \\ A_{\delta_k}=R_2Q_2+\delta_kR_LQ_1 \\ A_{kQ_{1\delta}}=R_2Q_2+k^2R_LQ_{1\delta} \\ B=R_L+R_2Q_2^2 \end{cases} \tag{21}$$

4.1. Transmission efficiency and optimal load

In SS topology, the transmission efficiency η applied compensation inductor conditions is derived by division of the active input and output power as follows.

$$\eta=\frac{k^2R_2R_LQ_1Q_2}{(R_2+R_L)(R_2+R_L+k^2R_2Q_1Q_2)} \tag{22}$$

Also, the optimal load in eq.(24) is obtained by applying the differential equation of eq.(23) to eq.(22).

$$\frac{\partial\eta}{\partial R_L}=0 \tag{23}$$

$$R_{opt}=R_2\sqrt{1+k^2Q_1Q_2} \tag{24}$$

For clear comprehension of the transmission characteristics based on formulas, the number of parameters is tried to reduce. By approximation about the Q factor in eq. (25), the transmission efficiency and the optimal load are simplified as eqs. (26) and (27). Since most compensation inductor possesses hundreds of Q factor, this approximation is appropriate.

$$Q=Q_1=Q_2,\ Q^2\gg 1 \tag{25}$$

$$\eta\simeq\frac{k^2R_2R_LQ^2}{(R_2+R_L)(R_2+R_L+k^2R_2Q^2)} \tag{26}$$

$$R_{opt}\simeq R_2\sqrt{1+k^2Q^2} \tag{27}$$

By eqs. (26) and (27), η_{max} of the maximum transmission efficiency satisfying the compensation inductor and the optimal load conditions is obtained as follows.

$$\eta_{max}\simeq\frac{k^2Q^2}{\left(1+\sqrt{1+k^2Q^2}\right)^2} \tag{28}$$

Other topologies are also analyzed in the same procedure, and the results are listed in Table 3 and Table 4. In Table 3, each similarity of the transmission efficiency in SS, PS topologies and in SP, PP topologies indicates that it is roughly determined by connection type of the secondary side inductor.

Table 3 Formulas of transmission efficiency in each topology

	$\eta\ (Q_1 \neq Q_2)$	$\eta\ (Q = Q_1 = Q_2, Q^2 \gg 1)$	η_{max}
SS topology	$\frac{k^2R_2R_LQ_1Q_2}{(R_2+R_L)(R_2+R_L+k^2R_2Q_1Q_2)}$	$\frac{k^2R_2R_LQ^2}{(R_2+R_L)(R_2+R_L+k^2R_2Q^2)}$	$\frac{k^2Q^2}{\left(1+\sqrt{1+k^2Q^2}\right)^2}$
SP topology	$\frac{\delta_kR_2R_LQ_1Q_{2\delta}^2Q_{2\delta}}{A_{\delta_k}R_2Q_2+B(A_{\delta_k}Q_2+R_L)}$	$\frac{\delta_kR_2R_LQ^4}{(R_L+R_2Q^2)(R_L+R_2Q^2+\delta_kR_LQ^2)}$	$\frac{\delta_kQ^2}{\left(1+\sqrt{1+\delta_kQ^2}\right)^2}$
PS topology	$\frac{\delta_kR_2R_LQ_{1\delta}Q_2}{(R_2+R_L)(R_2+R_L+\delta_kR_2Q_{1\delta}Q_2)}$	$\frac{\delta_kR_2R_LQ^2}{(R_2+R_L)(R_2+R_L+\delta_kR_2Q^2)}$	$\frac{\delta_kQ^2}{\left(1+\sqrt{1+\delta_kQ^2}\right)^2}$
PP topology	$\frac{k^2R_2R_LQ_{1\delta}Q_{2\delta}^2Q_{2\delta}}{A_{kQ_{1\delta}}R_2Q_2+B(A_{kQ_{1\delta}}Q_2+R_L)}$	$\frac{k^2R_2R_LQ^4}{(R_L+R_2Q^2)(R_L+R_2Q^2+k^2R_LQ^2)}$	$\frac{k^2Q^2}{\left(1+\sqrt{1+k^2Q^2}\right)^2}$

Table 4 Formulas of optimal load in each topology

	R_{Lopt} $(Q_1 \neq Q_2)$	R_{Lopt} $(Q = Q_1 = Q_2, Q^2 \gg 1)$
SS topology	$R_2\sqrt{1+k^2Q_1Q_2}$	$R_2\sqrt{1+k^2Q^2}$
SP topology	$\frac{R_2Q_2\sqrt{Q_2Q_{2\delta}}}{\sqrt{1+\delta_kQ^2}}$	$\frac{R_2Q^2}{\sqrt{1+\delta_kQ^2}}$
PS topology	$R_2\sqrt{1+\delta_kQ_{1\delta}Q_2}$	$R_2\sqrt{1+\delta_kQ^2}$
PP topology	$\frac{R_2Q_2\sqrt{Q_2Q_{2\delta}}}{\sqrt{1+k^2Q^2}}$	$\frac{R_2Q^2}{\sqrt{1+k^2Q^2}}$

η_{max} in all topologies closely resembles except for the difference between k^2 and δ_k. Considering $\delta_k \simeq k^2$ when the coupling coefficient is small, four compensation topologies achieve the same values of the maximum efficiency as follows.

$$\eta_{max}^{all} = \frac{k^2Q^2}{\left(1+\sqrt{1+k^2Q^2}\right)^2} \tag{29}$$

Based on this formula, the transition of the maximum efficiency with k, Q variation is calculated as shown in Fig. 4(a). The maximum efficiency increases with higher k, Q is understood.

In Table 4, each similarity of the optimal load in SS, PS topologies and in SP, PP topologies is confirmed, although it is clear from the similarity of the transmission efficiency. Assuming $\delta_k \simeq k^2$ for detailed evaluation, each optimal load in SS, PS topologies and in SP, PP topologies provides the same formulas as follows and shown in Fig 4(b) and (c).

$$R_{Lopt}^{SS,PS} = R_2\sqrt{1+k^2Q^2} \tag{30}$$

$$R_{Lopt}^{SP,PP} = \frac{R_2Q^2}{\sqrt{1+k^2Q^2}} \tag{31}$$

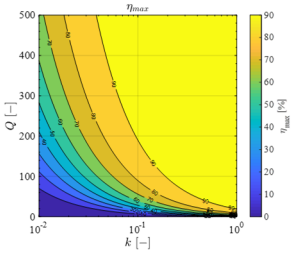

(a) η_{max}^{all}

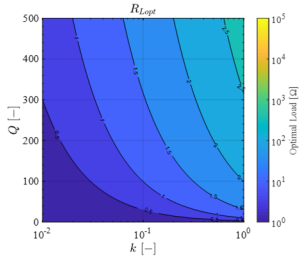

(b) $R_{Lopt}^{SS,PS}$

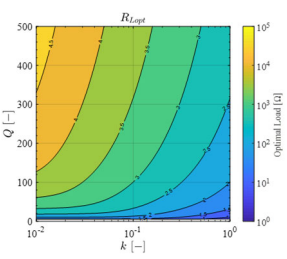

(c) $R_{Lopt}^{SP,PP}$

Fig. 4. Calculation results of efficiency and R_{Lopt} with k and Q variation based on approximated formulas

Based on these formulas, the transitions of the optimal load with k, Q variation are calculated as shown in Fig. 4(b), Fig. 4(c). Here, $R_2 = 1\ \Omega$ is considered. The optimal loads in SS and PS topologies increase with higher k, Q. Conversely, those in SP and PP topologies increase with lower k and higher Q. Furthermore, those in SP and PP topologies are considerably larger than those in SS and PS topologies. This difference is also confirmed from following proportional equation about the optimal load of each topology.

$$R_{Lopt}^{SS,PS} : R_{Lopt}^{SP,PP} = 1 + k^2Q^2 : Q^2 \simeq k^2 : 1 \tag{32}$$

Considering $k^2Q^2 \gg 1$ for high-efficiency transmission, the optimal load in SS, PS topologies are about k^2 times more than SP, PP topologies. This difference makes it possible to select the topology according to the load specification of the application.

4.2. Output power

In SS topology, the active output power P_{out} applied compensation inductor condition is derived as eq.(33). By approximation about the Q factor in eq.(25), the output power is simplified as eq.(34). By eqs.(27) and (34), $P_{out,\eta_{max}}$ of the output power satisfying the compensation inductor and the optimal load conditions is obtained as eq.(35).

$$P_{out} = \frac{k^2R_2R_LQ_1Q_2}{R_1(R_2+R_L+k^2R_2Q_1Q_2)}\left|\dot{V}_1\right|^2 \tag{33}$$

$$P_{out} \simeq \frac{k^2R_2R_LQ^2}{R_1(R_2+R_L+k^2R_2Q^2)^2}\left|\dot{V}_1\right|^2 \tag{34}$$

$$P_{out,\eta_{max}} \simeq \frac{\eta_{max}}{R_1\sqrt{1+k^2Q^2}}\left|\dot{V}_1\right|^2 \tag{35}$$

Other topologies are also analyzed in the same procedure, and the results are listed in Table 5. $P_{out,\eta_{max}}$ depend on η_{max}, $|\dot{V}_1|$ and $Z_{in,\eta_{max}}$ listed in Table 6. Also, $P_{out,\eta_{max}}$ in SS, SP topologies and in PS, PP topologies closely resemble. Assuming $\delta_k \simeq k^2$ for detailed evaluation, each output power in SS, SP topologies and in PS, PP topologies provides the same formulas as follows.

$$P_{out,\eta_{max}}^{SS,SP} = \frac{\eta_{max}}{R_1\sqrt{1+k^2Q^2}}\left|\dot{V}_1\right|^2 \tag{36}$$

$$P_{out,\eta_{max}}^{PS,PP} = \frac{\eta_{max}\sqrt{1+k^2Q^2}}{R_1Q^2}\left|\dot{V}_1\right|^2 \tag{37}$$

Based on these formulas, the transitions of the output power with k, Q variation are calculated as shown in Fig. 5(a), Fig.5(b). Here, $|\dot{V}_1| = 100$ V and $R_1 = 1\ \Omega$ are considered. The output power in SS and SP topologies increase with lower k, Q. Conversely, those in PS and PP topologies increase with higher k and lower Q. Furthermore, the range of high-power transmission in PS and PP topologies are considerably narrower than those in SS and SP topologies. This difference is also confirmed from following proportional equation about the output power of each topology.

$$P_{out,\eta_{max}}^{SS,SP} : P_{out,\eta_{max}}^{PS,PP} = Q^2 : 1 + k^2Q^2 \simeq 1 : k^2 \tag{38}$$

Considering $k^2Q^2 \gg 1$ for high-efficiency transmission, the output power of PS, PP topologies are about k^2 times more than SS, SP topologies for the same maximum efficiency. Therefore, SS and SP topologies are superior to PS and PP topologies. But SS and SP topologies require the couplers design with appropriate k to consider the trade-off between the transmission efficiency and output power.

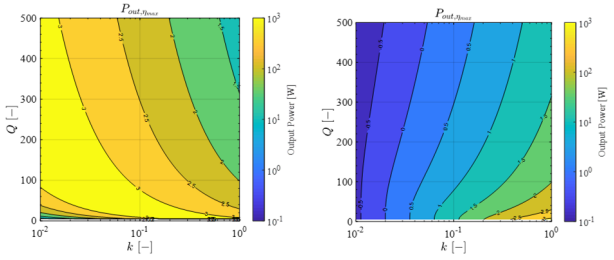

(a) $P_{out,\eta_{max}}^{SS,SP}$ (b) $P_{out,\eta_{max}}^{PS,PP}$

Fig. 5. Calculation results of power with k and Q variation based on approximated formulas

4.3. Input impedance

In SS topology, the input impedance Z_{in} applied compensation inductor condition is derived as eq.(39). By approximation about the Q factor in eq.(25), the input impedance is simplified as eq.(40). By eqs.(27) and (40), $Z_{in,\eta_{max}}$ of the input impedance satisfying the compensation inductor and the optimal load conditions is obtained as eq.(41).

$$Z_{in} = \frac{R_1(R_2+R_L+k^2R_2Q_1Q_2)}{R_2+R_L} \tag{39}$$

$$Z_{in} \simeq \frac{R_1(R_2+R_L+k^2R_2Q^2)}{R_2+R_L} \tag{40}$$

$$Z_{in,\eta_{max}} = R_1\sqrt{1+k^2Q^2} \tag{41}$$

Other topologies are also analyzed in the same procedure, and the results are listed in Table 6. The input impedances in SP, PS, PP topologies indicate a complex number, and the complete CUPF characteristics cannot be obtained. But, large Q factor approximates them to real number and CUPF characteristics is achieved.

Table 5 Formulas of output power in each topology

	$P_{opt}\ (Q_1 \neq Q_2)$	$P_{opt}\ (Q = Q_1 = Q_2, Q^2 \gg 1)$	$P_{out,\eta_{max}}$
SS topology	$\frac{k^2R_2R_LQ_1Q_2}{R_1(R_2+R_L+k^2R_2Q_1Q_2)^2}\lvert\dot{V_1}\rvert^2$	$\frac{k^2R_2R_LQ^2}{R_1(R_2+R_L+k^2R_2Q^2)^2}\lvert\dot{V_1}\rvert^2$	$\frac{\eta_{max}}{R_1\sqrt{1+k^2Q^2}}\lvert\dot{V_1}\rvert^2$
SP topology	$\frac{\delta_kR_2R_LQ_1Q_2^2Q_{2\delta}}{R_1\{A_{\delta_k}^2+(A_{\delta_k}Q_2+R_L)^2\}}\lvert\dot{V_1}\rvert^2$	$\frac{\delta_kR_2R_LQ^4}{R_1(R_L+R_2Q^2+\delta_kR_LQ^2)^2}\lvert\dot{V_1}\rvert^2$	$\frac{\eta_{max}}{R_1\sqrt{1+\delta_kQ^2}}\lvert\dot{V_1}\rvert^2$
PS topology	$\frac{\delta_kQ_2R_2R_L}{R_1Q_1(R_2+R_L)^2}\lvert\dot{V_1}\rvert^2$	$\frac{\delta_kR_2R_L}{R_1(R_2+R_L)^2}\lvert\dot{V_1}\rvert^2$	$\frac{\eta_{max}\sqrt{1+\delta_kQ^2}}{R_1Q^2}\lvert\dot{V_1}\rvert^2$
PP topology	$\frac{k^2R_2R_LQ_2^2Q_{2\delta}}{R_1Q_1(B^2+R_2^2Q_2^2)}\lvert\dot{V_1}\rvert^2$	$\frac{k^2R_2R_LQ^2}{R_1(R_L+R_2Q^2)^2}\lvert\dot{V_1}\rvert^2$	$\frac{\eta_{max}\sqrt{1+k^2Q^2}}{R_1Q^2}\lvert\dot{V_1}\rvert^2$

Table 6 Formula of input impedance in each topology

	$Z_{in}\ (Q_1 \neq Q_2)$	$Z_{in}\ (Q = Q_1 = Q_2,\ Q^2 \gg 1)$	$Z_{in,\eta_{max}}$
SS topology	$\frac{R_1(R_2+R_L+k^2R_2Q_1Q_2)}{R_2+R_L}$	$\frac{R_1(R_2+R_L+k^2R_2Q^2)}{R_2+R_L}$	$R_1\sqrt{1+k^2Q^2}$
SP topology	$\frac{R_1\{A_{\delta_k}+j(A_{\delta_k}Q_2+R_L)\}}{R_2Q_2+jB}$	$\frac{R_1(R_L+R_2Q^2+\delta_kR_LQ^2)}{R_L+R_2Q^2}$	$R_1\sqrt{1+\delta_kQ^2}$
PS topology	$\frac{R_1Q_1(R_2+R_L)(1+jQ_1)}{\delta_kR_2Q_2+j(R_2+R_L+\delta_kR_2Q_1Q_2)}$	$\frac{R_1Q^2(R_2+R_L)}{R_2+R_L+\delta_kR_2Q^2}$	$\frac{R_1Q^2}{\sqrt{1+\delta_kQ^2}}$
PP topology	$\frac{-jR_1Q_1(R_2Q_2+jB)(1+jQ_1)}{A_k+k^2R_LQ_2+j\{A_kQ_2+R_L(1-k^2)\}}$	$\frac{R_1Q^2(R_L+R_2Q^2)}{R_L+R_2Q^2+k^2R_LQ^2}$	$\frac{R_1Q^2}{\sqrt{1+k^2Q^2}}$

Table 7 Formula of input current and voltage in each topology

	$\lvert\dot{I_2}\rvert$	$\lvert\dot{I_2}\rvert_{max}$	CC range
SS topology	$\frac{k\sqrt{R_2Q_1Q_2}}{\sqrt{R_1}(R_2+R_L+k^2R_2Q_1Q_2)}\lvert\dot{V_1}\rvert$	$\frac{k\sqrt{Q_1Q_2}}{\sqrt{R_1R_2}(1+k^2Q_1Q_2)}\lvert\dot{V_1}\rvert$	$R_L \ll R_2(1+k^2Q_1Q_2)$
PP topology	$\frac{kQ_2\sqrt{R_2Q_{2\delta}}}{R_1Q_1(B^2+R_2^2Q_2^2)}\lvert\dot{V_1}\rvert$	$\frac{k}{\sqrt{R_1R_2Q_1Q_2}}\lvert\dot{V_1}\rvert$	$R_L \ll R_2Q_2\sqrt{Q_2Q_{2\delta}}$
	$\lvert\dot{V_2}\rvert$	$\lvert\dot{V_2}\rvert_{max}$	CV range
SP topology	$\frac{R_LQ_2\sqrt{\delta_kR_2Q_1Q_{2\delta}}}{\sqrt{R_1\{A_{\delta_k}^2+(A_{\delta_k}Q_2+R_L)^2\}}}\lvert\dot{V_1}\rvert$	$\frac{Q_2\sqrt{\delta_kR_2Q_1Q_{2\delta}}}{\sqrt{R_1(1+\delta_kQ_1Q_2+\delta_k^2Q_1^2)}}\lvert\dot{V_1}\rvert$	$\frac{R_2Q_2\sqrt{Q_2Q_{2\delta}}}{\sqrt{\delta_k^2Q_1^2+(1+\delta_kQ_1Q_2)^2}} \ll R_L$
PS topology	$\frac{R_L\sqrt{\delta_kR_2Q_2}}{\sqrt{R_1Q_1}(R_2+R_L)}\lvert\dot{V_1}\rvert$	$\sqrt{\frac{\delta_kR_2Q_2}{R_1Q_1}}\lvert\dot{V_1}\rvert$	$R_2 \ll R_L$

4.4. Output current and voltage

This section provides the analysis procedures of output current and voltage for CC and CV characteristics.

CC characteristics: In SS topology, the output current $|\dot{I}_2|$ applied compensation inductor condition is derived as follows.

$$\frac{k\sqrt{R_2Q_1Q_2}}{\sqrt{R_1}(R_L+R_2+k^2R_2Q_1Q_2)}|\dot{V}_1| \tag{42}$$

Unlike previous analysis, complete CC characteristics cannot be obtained since $|\dot{I}_2|$ are functions of R_L. But it is obtained with maximum current value $|\dot{I}_2|_{max}$ when $R_L = 0$ as in eq. (43). Here, this paper defines the load range with the small attenuation of output current up to $1/2$ times the maximum value as the following CC range.

$$|\dot{I}_2|_{max} = \frac{k\sqrt{Q_1Q_2}}{\sqrt{R_1R_2}(1+k^2Q_1Q_2)}|\dot{V}_1| \tag{43}$$

$$\text{CC range}: R_L \ll R_2(1+k^2Q_1Q_2) \tag{44}$$

If R_{Lopt} as the design value satisfies the above range sufficiently, CC characteristics can be achieved.

CV characteristics: In SP topology, the output voltage $|\dot{V}_2|$ applied compensation inductor condition is derived as follows.

$$|\dot{V}_2| = \frac{R_LQ_2\sqrt{\delta_kR_2Q_1Q_{2\delta}}}{\sqrt{R_1\{A_{\delta_k}^2+(A_{\delta_k}Q_2+R_L)^2\}}}|\dot{V}_1| \tag{45}$$

Unlike previous analysis, complete CV characteristics cannot be obtained since $|\dot{V}_2|$ are functions of R_L. But, it is obtained with maximum voltage value $|\dot{V}_2|_{max}$ when $R_L = \infty$ as in eq.(46). Here, this paper defines the load range with the small attenuation of output voltage up to $1/2$ times the maximum value as the following CV range.

$$|\dot{V}_2|_{max} \simeq \frac{Q_2\sqrt{\delta_kR_2Q_1Q_{2\delta}}}{\sqrt{R_1(1+\delta_kQ_1Q_2+\delta_k^2Q_1^2)}}|\dot{V}_1| \tag{46}$$

$$\text{CV range}: \frac{R_2Q_2\sqrt{Q_2Q_{2\delta}}}{\sqrt{\delta_k^2Q_1^2+(1+\delta_kQ_1Q_2)^2}} \ll R_L \tag{47}$$

If R_{Lopt} as the design value satisfies the above conditions sufficiently, CV characteristics can be achieved.

Other topologies are also analyzed in the same procedure, and the results are listed in Table 7. The output current or voltage of all topologies depend on R_L, but SS and PP topologies obtain CC characteristics by satisfying CC ranges. Conversely, SP and PS topologies obtain CV characteristics by satisfying CV ranges. Including CUPF characteristic, the gyrator characteristic is obtained in SS, PP topologies, and the ideal transformer characteristics is obtained in SP, PS topologies.

5. Experiment Verification

The effectiveness of the design conditions and evaluation of the transmission characteristics are verified by the circuit calculation and powering experiment. Also, this paper deals with only SS and SP topologies where relatively high power is expected. The calculation conditions are the same as the experimental conditions described below.

The experimental equipment shown in Fig. 6 consists of the four copper plates for CPT couplers, compensation inductors, compensation capacitors, pure resistive loads, and an AC constant voltage source. The copper plates are arranged horizontally as Fig. 1 with the size and configuration listed in Table 8. The plate depth is t [mm]. The AC constant voltage source is composed of a function generator (Tektronix AFG3022) and bipolar amplifier (NF HSA4014). Also, the parameters of each element are measured by the impedance analyzer and listed in Table 9. According to a March 15, 2016 revised ministerial ordinance within Japan, the frequencies for consumer products as the 400 kHz band, have been added as type designations for the CPT. Therefore, 400 kHz is selected here. In this experiment, the self-capacitances of the CPT couplers are very small. This requires the inductors with the larger inductances to resonate at the low frequency of 400 kHz, resulting in the significant decrease in output power. Thus, the external capacitors with C_{ex1}, C_{ex2} are connected in parallel to the CPT couplers to compensate for the self-capacitances of the system as follows.

$$C_{1,2} = C_{in1,2} + C_{ex1,2} \tag{48}$$

The input and output voltages $\dot{V}_1$, $\dot{V}_2$, currents $\dot{I}_1$, $\dot{I}_2$ are measured by the oscilloscope, differential probes and current probes. The active input and output powers P_{in}, P_{out} are gained by averaging product of the instantaneous voltages and currents using math function of oscilloscope. Also, input power factor is measured by the impedance analyzer.

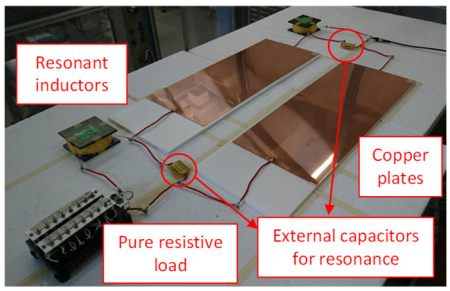

Fig. 6. Experimental equipment of CPT system

Table 8 Plate size and configuration parameters

l_1 [mm]	l_2 [mm]	t [mm]	w [mm]	g [mm]
250	600	0.4	70	7

Table 9 Experimental conditions

	SS topology	SP topology
C_{in1}/C_{in2} [pF]	100.7 / 99.8	
C_{ex1}/C_{ex2} [pF]	777.9 / 777.1	
C_1/C_2 [pF]	878.6 / 876.8	
C_m [pF]	88.6	
k [−]	0.1	
f [kHz]	400	
V_1 [V]	10	
L_1/L_2 [μH]	182.0 / 182.4	179.8 / 182.4
R_1/R_2 [Ω]	1.5 / 1.5	1.7 / 1.5
Q_1/Q_2 [−]	307.7 / 312.5	267.9 / 312.5

The calculation and experimental results of the load characteristics of η, P_{out}, $\cos\theta_{in}$, $|\dot{I}_2|$ in SS topology and $|\dot{V}_2|$ in SP topologies are shown in Fig. 7. About the η, $|\dot{I}_2|$ and $|\dot{V}_2|$, the experimental results match the calculation results. Fig. 7(a) shows that the maximum efficiency is achieved at the optimal load in both topologies. Fig. 7(d) shows that SS topology possesses CC characteristics and SP topology possesses CV characteristics at the load variation around the optimal load. Conversely, the results of P_{out} and $\cos\theta_{in}$ are slightly difference. Even the calculation results of the input power factor do not achieve $\cos\theta_{in} = 1$. This is because the parasitic capacitances of the differential probes at the measurement which cannot be ignored cause the resonance deviation.

In addition, the designed optimal loads and transmission characteristics with those η_{max}, $P_{out,\eta_{max}}$, $\cos\theta_{in,\eta_{max}}$ are summarized in Table 10. Unlike the results of the load characteristics, the experimental results matches the calculation results in not only η_{max} but also $P_{out,\eta_{max}}$ and $\cos\theta_{in,\eta_{max}}$. This implies the robustness to the parameter error at the optimal load in transmission characteristics. Table 10 shows the optimal load in SP topology is about 109 times the SS topology, which is roughly $1/k^2$ times. Also, SS and SP topologies gain the

equivalent maximum efficiency and output power at that time, and unit power factor of source. Therefore, excluding the error due to the resonance shift, the effectiveness of the design conditions and evaluation of the transmission characteristics are verified.

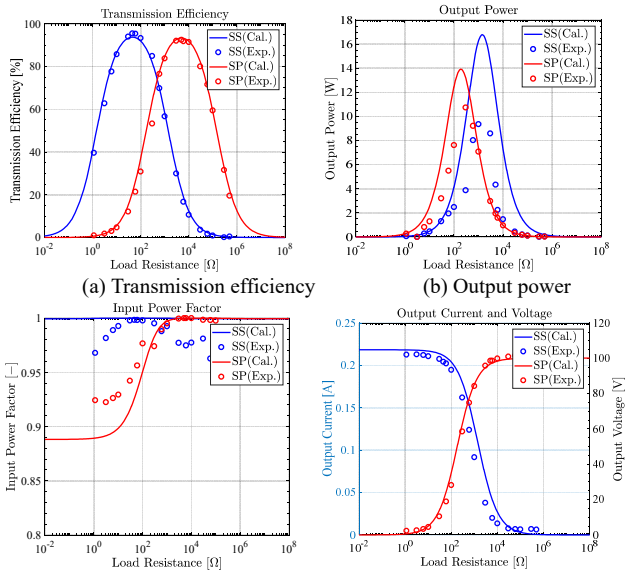

(a) Transmission efficiency (b) Output power

(c) Input power factor (d) Output current and voltage

Fig. 7. Calculation and experimental results of transmission characteristics with load variation

Table 10 Calculation and experimental result

	SS topology		SP topology	
	cal.	exp.	cal.	exp.
R_{Lopt} [Ω]	45.4		4956	
η_{max} [%]	92.3	95.5	93.3	92.5
$P_{out,\eta_{max}}$ [W]	1.96	1.94	1.88	1.94
$\cos\theta_{in,\eta_{max}}$ [−]	1.0	1.0	1.0	1.0

6. Conclusion

This paper analyzed and evaluated the transmission characteristics in the four of SS, SP, PS and PP topologies applied the compensation inductors and the optimal load conditions based on the gyrator and ideal transformer design. The voltage source is used uniformly. Under the unified design conditions, four topologies can obtain the same transmission efficiency and the CUPF characteristics of source. However, there are the differences which the output power of PS, PP topologies is about k^2 times smaller than that in SS, SP topologies, and the optimal load in SS and PS topologies is about k^2 times smaller than that in SP and PP topologies. Also, SS and PP topologies showed CC characteristics, and SP and PS topologies showed CV characteristics. Furthermore, in only SS and SP topologies with high power, the effectiveness of the design method and transmission characteristics evaluation is verified by the powering experiment. From the above evaluations, either SS or SP topologies which are superior in terms of the output power should be selected according to relationship between the optimal load value, CC or CV characteristics and specification of the applications when power source is voltage source. The future work is to achieve the high-efficiency and high-power transmission at the long distance in CPT in SS and SP topologies.

Acknowledgment

This work was partly supported by JSPS KAKENHI Grant Number 17H04915.

References

(1) A. Kurs, A. Karalis, R. Moffatt, J. D. Joannopoulos, P. Fisher, and M. Soljačić, "Wireless power transfer via strongly coupled magnetic resonances," *sci.*, vol. 317, no. 5834, pp. 83–86, 2007.

(2) T. Imura and Y. Hori, "Maximizing air gap and efficiency of magnetic resonant coupling for eireless power transfer using equivalent circuit and neumann formula," *IEEE Trans. Ind. Electron.*, vol. 58, no. 10, pp.4746–4752, 2011.

(3) G. A. Covic and J. T. Boys, "Modern trends in inductive power transfer for transportation applications," *IEEE J. Emerg. Sel. Topics Power Electron.*, vol. 1, no. 1, pp. 28–41, 2013.

(4) M. P. Theodoridis, "Effective capacitive power transfer," *IEEE Trans. Power Electron.*, vol. 27, no. 12, pp. 4906–4913, 2012.

(5) C. Liu, A. P. Hu, and N. C. Nair, "Modelling and analysis of a capacitively coupled contactless power transfer system," *IET Power Electron.*, vol. 4, no. 7, pp. 808–815, 2011.

(6) A. Kumar, S. Pervaiz, C.-K. Chang, S. Korhummel, Z. Popovic, and K. K. Afridi, "Investigation of power transfer density enhancement in large air-gap capacitive wireless power transfer systems," in *2015 IEEE Wireless Power Transfer Conference (WPTC)*, pp. 1–4, 2015.

(7) A. P. Hu, C. Liu, and H. L. Li, "A novel contactless battery charging system for soccer playing robot," in *Mechatronics and Machine Vision in Practice, 2008. M2VIP 2008. 15th International Conference on*, pp.646–650, 2008.

(8) S. Doron, O. Shaul, and M. E. Mehrdad, "A resonant led driver with capacitive power transfer," in *2014 IEEE Applied Power Electronics Conference and Exposition - APEC 2014*, pp. 1384–1387, 2014.

(9) R. Jegadeesan, K. Agarwal, Y.-X. Guo, S.-C. Yen, and N. V. Thakor, "Wireless power delivery to flexible subcutaneous implants using capacitive coupling," *IEEE Trans. Microw. Theory Techn.*, vol. 65, no. 1, pp.280–292, 2017.

(10) J. Dai, S. Hagen, D. C. Ludois, and I. P. Brown, "Synchronous generator brushless field excitation and voltage regulation via capacitive coupling through journal bearings," *IEEE Trans.Ind. Appl.*, vol. 53, no. 4, pp. 3317–3326, 2017.

(11) N. Sakai, D. Itokazu, Y. Suzuki, S. Sakihara, and T. Ohira, "One-kilowatt capacitive power transfer via wheels of a compact electric vehicle," in *Wireless Power Transfer Conference (WPTC), 2016 IEEE*, pp. 1–3, 2016.

(12) J. Dai and D. C. Ludois, "A survey of wireless power transfer and a critical comparison of inductive and capacitive coupling for small gap applications," *IEEE Trans. Power Electron.*, vol. 30, no. 11, pp. 6017–6029, 2015.

(13) F. Lu, H. Zhang, H. Hofmann, and C. Mi, "A double-sided lclc- compensated capacitive power transfer system for electric vehicle charg- ing," *IEEE Trans. Power Electron.*, vol. 30, no. 11, pp. 6011–6014, 2015.

(14) H. Umegami, M. Ishihara, F. Hattori, M. Masuda, M. Yamamoto, and K. Umetani, "Mid-range khz electric resonance coupling wireless power tranfser," in *Energy Conversion Congress and Exposition (ECCE), 2015 IEEE*, pp. 3197–3202, 2015.

(15) S. Kenta, I. Takehiro, and Y. Hori, "Experimental verification of optimal load to achieve maximum efficiency in capacitive power transfer with resonance coupling," in *IEICE Asian Wireless Power Transfer Workshop (AWPT)*, 2017.

(16) K. Suzuki, K. Hata, T. Imura, and Y. Hori, "Ss and sp topology analysis for capacitive power transfer with resonance coupling based on power factor consideration," in *IECON 2018 - 44th Annual Conf. of the IEEE Industrial Electron. Society*, pp. 4846–4851, 2018.

(17) F. Lu, H. Zhang, H. Hofmann, and C. C. Mi, "A double-sided lc-compensation circuit for loosely coupled capacitive power transfer," *IEEE Trans. Power Electron.*, vol. 33, no. 2, pp. 1633–1643, 2018.

(18) T. Komaru and H. Akita, "Positional characteristics of capacitive power transfer as a resonance coupling system," in *IEEE Wireless Power Transfer (WPT)*, pp. 218–221, 2013.

(19) Y. H. Sohn, B. H. Choi, E. S. Lee, G. C. Lim, G.-H. Cho, and C. T.Rim, "General unified analyses of two-capacitor inductive power transfer systems: Equivalence of current-source ss and sp compensations," *IEEE Trans. Power Electron*, vol. 30, no. 11, pp. 6030–6045, 2015.

(20) Y. H. Sohn, B. H. Choi, G.-H. Cho, and C. T. Rim, "Gyrator-based analysis of resonant circuits in inductive power transfer systems," *IEEE Trans. Power Electron.*, vol. 31, no. 10, pp. 6824–6843, 2016.

(21) Hisaichi Irie, Tomohiro Yabuuchi, "High-frequency constant-current power supply in noncontact energy transfer system using immittance converter"., Electrical Engineering in Japan., 2007, Vol.158, No.3, p.81.

(22) H. Zhang, F. Lu, H. Hofmann, W. Liu, and C. C. Mi, "A four-plate compact capacitive coupler design and lcl-compensated topology for capacitive power transfer in electric vehicle charging application," *IEEE Trans. Power Electron.*, vol. 31, no. 12, pp. 8541–8551, 2016.

Takehiro Imura

(Member) received the bachelor's degree in electrical and electronics engineering from Sophia University, Tokyo, Japan, in 2005, and the M.E. degree in electronic engineering and the D.Eng. degree in electrical engineering from The University of Tokyo, Tokyo, in 2007 and 2010, respectively. He joined the Department of Advanced Energy, Graduate School of Frontier Sciences, University of Tokyo, as a Research Associate, where since 2015, he has been a Project Lecturer. In 2019, he joined the Department of Electrical Engineering, Tokyo University of Science, as an Associate Professor. He is currently investigating wireless power transfer using magnetic resonant coupling and electric resonant coupling. His research interests include electric vehicle in-motion connected to renewable energy, sensors and cancer treatment. He is the winner of the IEEJ Industry Applications Society Distinguished Transaction Paper Award in 2015, of the IEEE Power Electronics Transactions First Prize Paper Award in 2017. He is a member of the Institute of Electrical and Electronics Engineers (IEEE), the Institute of Electronics, Information and Communication Engineers (IEICE), and the Society of Automotive Engineers of Japan (JSAE).

Kenta Suzuki

(Non-Member) received the B.S. from Chiba University and M.S. from the University of Tokyo, Japan in 2017 and 2019, respectively.

Katsuhiro Hata

(Member) received the M.S. and Ph.D. degrees from the University of Tokyo in 2015 and 2018, respectively. He is currently a Research Associate with the Department of Informatics and Electronics, Institute of Industrial Science, the University of Tokyo. His research interests include power electronics, wireless power transfer, and e-mobility for transportation. He is a member of the Institute of Electrical and Electronics Engineers, the Institute of Electronics, Information and Communication Engineers, and the Society of Automotive Engineers of Japan.

Yoichi Hori

(Fellow) received the B.S., M.S., and Ph.D. degrees in electrical engineering from the University of Tokyo, Tokyo, Japan, in 1978, 1980, and 1983, respectively. In 2000, he became a Professor at the University of Tokyo, and where in 2008, he moved to the Department of Advanced Energy, Graduate School of Frontier Sciences. His research fields are control theory and its industrial applications in motion control, mechatronics, robotics, and electric vehicles. He is the winner of the Best Transactions Paper Award from the IEEE Transactions on Industrial Electronics in 1993, 2001 and 2013, of the 2000 Best Transactions Paper Award from IEEJ, and 2011 Achievement Award of IEEJ. He is IEEE Life Fellow and a past AdCom member of IES. He has been the Treasurer of the IEEE Japan Council and Tokyo Section in a few years since 2001. He is now IEEJ Fellow and JSAE Fellow, and also a member of the Society of Instrument and Control Engineers, Robotics Society of Japan, Japan Society of Mechanical Engineers, and so on. He was the President of the Industry Applications Society of the IEEJ, and the President of WEVA (World Electric Vehicle Association), and the Director of Japan Automobile Research Institute (JARI).